

## RESEARCH ARTICLE

## Carbonate chemistry seasonality in a tropical mangrove lagoon in La Parguera, Puerto Rico

Erick M. García-Troche<sup>1,2\*</sup>, Julio M. Morell<sup>1,2</sup>, Melissa Meléndez<sup>3</sup>, Joseph E. Salisbury<sup>4</sup>

**1** Department of Marine Sciences, University of Puerto Rico at Mayagüez, Mayagüez, Puerto Rico, **2** Caribbean Coastal Ocean Observing System, NOAA-IOOS, Lajas, Puerto Rico, **3** School of Ocean and Earth Science and Technology (SOEST), University of Hawai'i at Manoa, Honolulu, Hawai'i, United States of America, **4** Ocean Process Analysis Laboratory, Institute for the Study of Earth, Oceans, and Space, University of New Hampshire, Durham, New Hampshire, United States of America

\* [erick.garcia1@upr.edu](mailto:erick.garcia1@upr.edu)

## Abstract

We investigated the seasonal carbonate chemistry variability within a semi-enclosed tropical mangrove lagoon in southwestern Puerto Rico. Biweekly measurements of seawater temperature, salinity, total alkalinity (TA), and dissolved inorganic carbon (DIC) were conducted from 2014 to 2018. We describe the possible mechanisms driving the observed variability by correlating the DIC/TA ratio with pH and  $\Omega_{\text{arg}}$ , suggesting that the mean pH ( $7.87 \pm 0.09$ ) and aragonite saturation state ( $\Omega_{\text{arg}}$ ,  $2.96 \pm 0.47$ ) of the mangrove lagoon negatively affected calcification. The measured  $p\text{CO}_2$  and DIC/TA ratios indicate that heterotrophic activity was the primary driver for persistent acidification, which reached its maximum expression during the wet season. We conclude that mangrove lagoons with limited seawater exchange and high carbon input will not mitigate ocean acidification.

## OPEN ACCESS

**Citation:** García-Troche EM, Morell JM, Meléndez M, Salisbury JE (2021) Carbonate chemistry seasonality in a tropical mangrove lagoon in La Parguera, Puerto Rico. PLoS ONE 16(5): e0250069. <https://doi.org/10.1371/journal.pone.0250069>

**Editor:** Kay C. Vopel, Auckland University of Technology, NEW ZEALAND

**Received:** November 13, 2019

**Accepted:** March 30, 2021

**Published:** May 5, 2021

**Copyright:** © 2021 García-Troche et al. This is an open access article distributed under the terms of the [Creative Commons Attribution License](https://creativecommons.org/licenses/by/4.0/), which permits unrestricted use, distribution, and reproduction in any medium, provided the original author and source are credited.

**Data Availability Statement:** All relevant data are within the manuscript and its [Supporting Information](#) files.

**Funding:** This research was funded by NOAA's Ocean Acidification Program. Support was also provided by US IOOS through the Caribbean Coastal Ocean Observing System (<https://www.caricoos.org>), Grant NA16NOS0120026. Both awards were granted to JMM. The funders had no role in study design, data collection, and analysis,

## Introduction

There is an increasing research interest to identify ecosystems where vulnerable species could persist under foreseen future scenarios, including high atmospheric carbon dioxide ( $\text{CO}_2$ ) concentrations and seawater temperatures [1]. Surface oceans have already warmed [2, 3] and acidified worldwide at an unprecedented pace [4], and scientists expect such trends to continue based on the Intergovernmental Panel on Climate Change (IPCC)  $\text{CO}_2$  emission scenarios [5].

Studies suggest that different coastal ecosystems, such as seagrass beds [6] and mangroves [7, 8], can mitigate ocean acidification (OA) driven by oceanic uptake of anthropogenic  $\text{CO}_2$ . A buffering effect may occur when “alkalinity increases the  $\text{CO}_2$  uptake capacity of seawater by neutralizing  $\text{H}^+$  ions and buffering the pH change associated with  $\text{CO}_2$  inputs” [9]. Seagrass ecosystems buffer OA at shallow depths and reduced water mass turnover [10, 11] by raising the pH and calcium carbonate ( $\text{CaCO}_3$ ) saturation while they are in a state of net autotrophy [10]. The buffering effect may be limited to specific periods throughout the year [12] and could have the opposite effect by exacerbating OA in the future [13].

A Caribbean mangrove system (St. John, United States Virgin Islands) was recently identified as a potential refuge from OA, upper-ocean warming, and solar radiation for non-reef

decision to publish, or preparation of the manuscript.

**Competing interests:** The authors have declared that no competing interests exist.

scleractinian coral species [8]. The authors suggested that  $\text{CaCO}_3$  sediment dissolution could have increased downstream total alkalinity (TA) to prevent OA from exacerbating [8]. Moreover, a study in an Australian mangrove creek suggested that mangrove sites could generate alkalinity via sulfate reduction and exported to nearby coastal areas, creating a zone buffered against OA [7]. Other studies suggest that mangrove ecosystems can pre-condition corals to low pH's [14] and serve as reservoirs for already tolerant coral species [15, 16].

Mangrove communities are known for their high productivity [17, 18] and are more productive than most terrestrial and marine communities [19]. However, global budgets still fail to fully quantify the amount of carbon fixated by mangrove vegetation, given that datasets and estimates on wood production and belowground allocation are limited [20]. Estimates note that inorganic carbon produced by mineralization activity could account for the missing carbon in global budgets, given that mineralization rates are severely underestimated [20]. Sulfate reduction and aerobic respiration are commonly the dominant metabolic pathways within tropical mangrove sediments [7, 21, 22]. The former yields alkalinity, assuming that the resulting sulfide is not re-oxidized to sulfate [23]. Coupled denitrification/nitrification and ammonification are restricted pathways in tropical mangrove environments due to scarce oxygen availability [24–26].

Studies published to date provide a good understanding of the carbonate chemistry diel variability at these mangrove sites [7, 8, 14–16]. However, the buffering role of mangroves at seasonal time scales remains unclear. This study's main objective is to determine if the tropical mangrove lagoon located on the southwest coast of Puerto Rico can buffer OA. We also aim to assess TA's seasonal variability, dissolved inorganic carbon (DIC), and physical dynamics (temperature, salinity, precipitation, tides, and winds). We hypothesize that mangrove lagoons with high mangrove carbon mineralization activity and limited flushing provide conditions that promote OA and reduce the aragonite saturation state ( $\Omega_{\text{arg}}$ ).

## Methods

### Site description

The study area is within La Parguera Marine Reserve, an estuary in which evaporation exceeds freshwater influx [27], located on the southwestern coast of Puerto Rico (Fig 1). The Reserve's cays, submerged reefs, and mangroves ecosystems surround and protect La Parguera town (17.974 °N, 67.046 °W) from intense wave energy. The wet season extends from August to November, while semiarid conditions prevail during the rest of the year (dry season). The Caribbean Surface Water, which constitutes the oceanic end-member for La Parguera, is a mixture of Tropical North Atlantic surface waters and continental river waters [28]. River plumes from the Amazon and Orinoco Rivers impinge in the region [29, 30], with maximum influence from June through October [33, 34]. The area is under the influence of easterly trade winds and a diurnal tide (S1 Fig) of small amplitude (ca. 0.3 meters).

The SE station (17.870 °N, 67.021 °W) is approximately 11 km off the coast of La Parguera and 1 km off the insular shelf-edge (Fig 1). This station represents the oceanic reference end-member.

The BB station (17.972 °N, 67.014 °W) is within The Bioluminescent Bay (Fig 2), 3.2 km east of La Parguera town (Fig 1). The Bioluminescent Bay has a 0.19 km<sup>2</sup> surface area, an average depth of 3.5 m [31], and a maximum of 4.5 m [32]. A 25-meter-wide red mangrove (*Rhizophora mangle* L.) fringe surrounds the bay and is a significant organic carbon source. The total estimated primary productivity for *R. mangle* in La Parguera was 3.85 g dry wt m<sup>-2</sup> day<sup>-1</sup>, while the litterfall fraction was in the 0.15 to 0.91 g dry wt m<sup>-2</sup> day<sup>-1</sup> range with a marked seasonal variability [33]. The BB water column's net community production has been reported to range

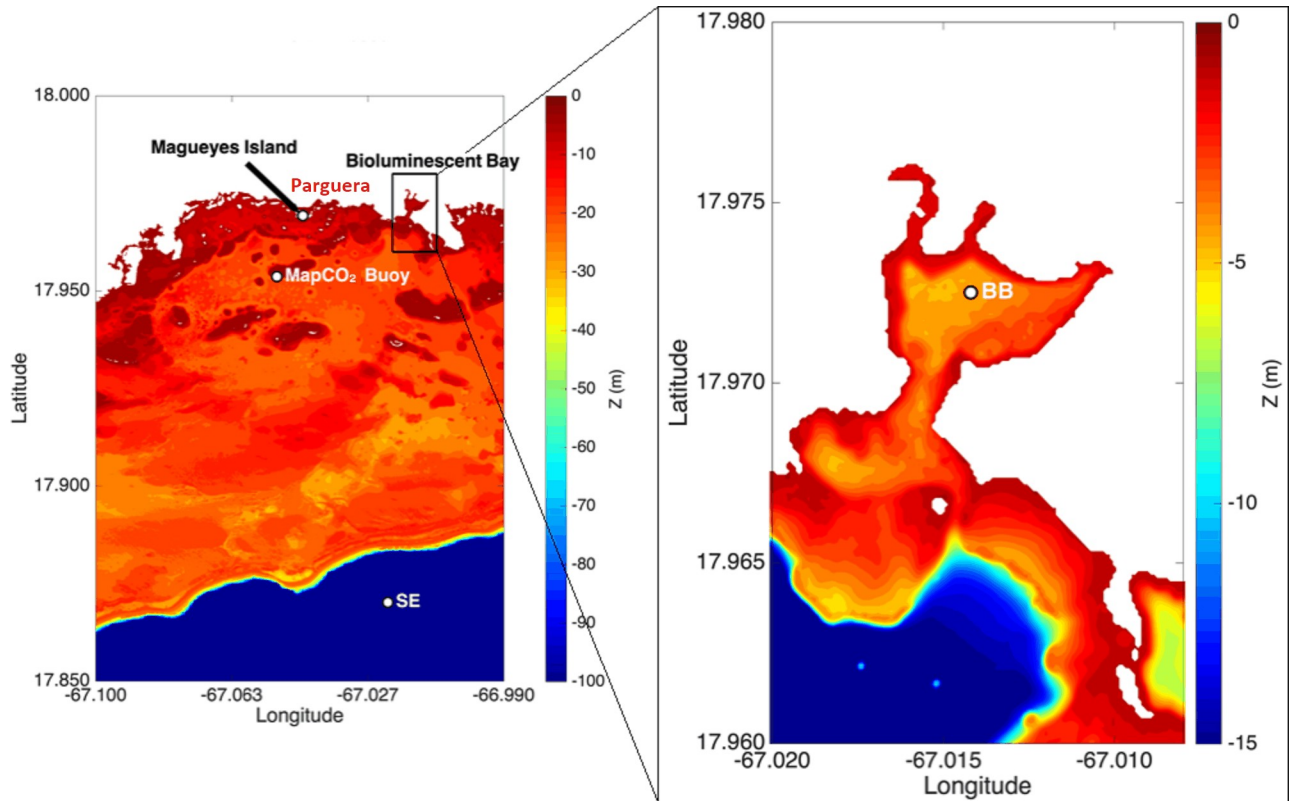


**Fig 1. Bathymetric maps of La Parguera Marine Reserve (Lajas, PR) and study sites.** La Parguera Marine Reserve is on the left panel. The white dots represent the shelf-edge station (SE), the moored autonomous carbon dioxide partial pressure (MapCO<sub>2</sub>) buoy, and the Marine Station (Magueyes Island). The Bioluminescent Bay is to the right, and the white dot represents the sampled station (BB). Note the corresponding depth color legend to the right of each map.

<https://doi.org/10.1371/journal.pone.0250069.g001>

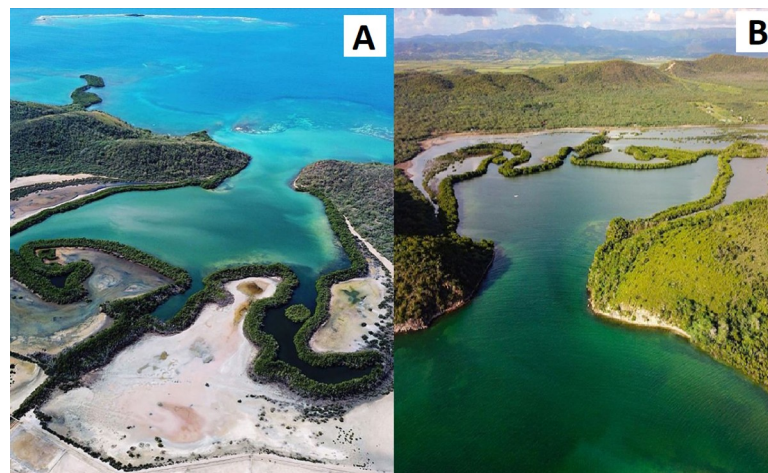


**Fig 2. Drone pictures of The Bioluminescent Bay.** The picture to the left (A, by Jonathan Vegilla) was shot from the north during the dry season. The picture on the right (B, by Omar López) was taken from the south during the wet season. Note the salt flats to the north of the bay, mostly dry in (A) and flooded in (B).

<https://doi.org/10.1371/journal.pone.0250069.g002>

from  $-5.99$  to  $-2.49$   $\text{g C m}^{-2} \text{ day}^{-1}$  [34, 35]. The bathymetry has an irregular shape with a narrow and shallow outlet to nearby shelf waters and a sill (1 m depth) at the entrance, limiting exchange with outer waters and shelters from wave energy [32, 36]. Most of the bottom comprises muddy sediments (ca. 7.5% grams of organic carbon content per gram of sediment, down to a 20 cm depth [37]). While coral reef systems are not known to exist within the bay, small coral communities live 200 meters beyond its entrance. Runoff from salt flats to the north of the bay flows into the lagoon via three channels during infrequent heavy rain periods. The lagoon is partially sheltered from the prevailing trade winds by mangroves and hills on its outlet's east and west sides.

## Fieldwork

Surveys were conducted every two weeks at SE (June 2014 to May 2018) and at BB (June 2014 to May 2015, October 2016 to May 2018) stations at approximately 8:00 and 9:00 AM local time, respectively. At times, we altered sampling frequency due to unfavorable weather conditions or instrument failure. Sampling depth at the SE station was 4 m, while at BB, it was 3 m. No permits were required to conduct this fieldwork.

Our data set includes DIC and TA measurements from discrete seawater samples, drawn from a 2.2 L Van Dorn sampler into 250 (or 125) mL borosilicate glass bottles and secured using greased stoppers, following the guide for best practices for  $\text{CO}_2$  measurements [38]. Each sample was fixed immediately with 0.02% of the total bottle volume using a saturated solution of mercury chloride ( $\text{HgCl}_2$ ) or immediately after returning to the laboratory (same day) to prevent biological alteration and stored at room temperature for later analysis. Each bottle was tightly sealed with about 1% of headspace to prevent atmospheric gas exchange. Analyses were performed within six months after sampling. Profile measurements of temperature and salinity were taken using an SBE25<sup>®</sup> conductivity, temperature, and depth recorder (CTD).

## Meteorological and tidal observations

Wind observations (Fig 3A) were obtained from a meteorological station [39] at the UPRM's Magueyes Island (Fig 1). The station is 3.1 km west of the BB site. We obtained daily accumulated precipitation observations (Fig 3B) collected at Magueyes Island from NOAA's National Center of Environmental Information [39]. Seasonality at La Parguera is clearly defined by precipitation patterns on a climatological scale and throughout the sampling period (2014–2018). Sea-level data for La Parguera is available from a NOAA tide gauge (station number 9759110) located in the west-end of Magueyes Island [40].

## Carbonate chemistry analyses and calculations

From June 2014 to May 2017, seawater samples for TA were analyzed at the University of New Hampshire (UNH) Ocean Processes Analysis Laboratory. TA analyses followed the Gran titration method [41], using an Apollo SciTech automated titrator and 0.1 N hydrochloric acid (HCl) titrant. The Orion 3-Star pH electrode (Thermo Fisher Inc.) was calibrated using low ionic strength pH buffers (certified on the U.S. National Bureau of Standards Scale to  $\pm 0.01$ ). Dickson's Certified Reference Materials (CRM) [42] were used to standardize the HCl titrant and validate the results. The precision and accuracy of the TA method as implemented at UNH were  $\pm 2$   $\mu\text{mol kg}^{-1}$  and  $\pm 3$ – $4$   $\mu\text{mol kg}^{-1}$ , respectively. A CRM was analyzed at the beginning and end of each run to correct for any potential drift. From June 2017 to May 2018, TA samples were analyzed at the University of Puerto Rico Mayagüez Campus (UPRM), Department of Marine Sciences, following the method described above and using similar

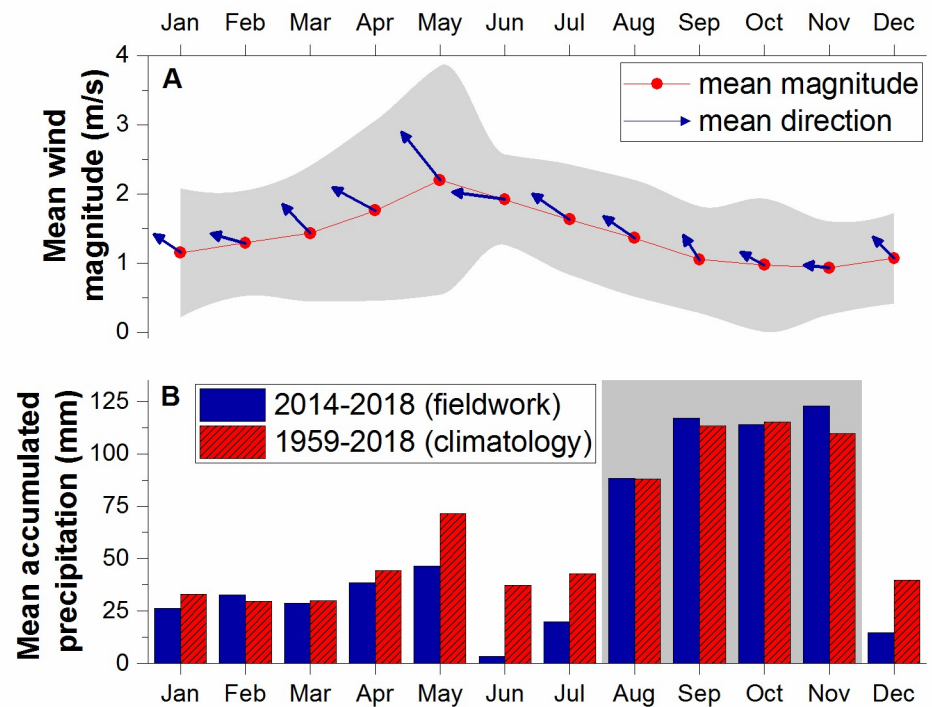


**Fig 3. Monthly mean weather conditions at La Parguera.** The upper graph (A) shows the mean wind magnitude for each month during the sampling period, where the gray area depicts one standard deviation of the wind magnitude. The lower graph (B) shows the mean accumulated precipitation during the sampling period (blue) and the climatology (red), where the gray area depicts the wet season.

<https://doi.org/10.1371/journal.pone.0250069.g003>

instrumentation. The precision and accuracy of the TA method as implemented at UPRM were  $\pm 2 \mu\text{mol kg}^{-1}$  and  $\pm 3\text{--}4 \mu\text{mol kg}^{-1}$ , respectively. We note that the TA samples from BB may include contributions from organic compounds [43], which we did not account for in this experiment.

All DIC samples were analyzed at UNH by measuring the infrared absorption of the  $\text{CO}_2$  released upon the sample's acidification with 10% phosphoric acid using an Apollo SciTech AS-C2 automated analyzer. CRM's were also used to calibrate the instrument. The precision and accuracy of the DIC method as implemented were  $\pm 2 \mu\text{mol kg}^{-1}$  and  $\pm 5 \mu\text{mol kg}^{-1}$ , respectively.

We calculated the seawater  $\text{CO}_2$  partial pressure ( $p\text{CO}_2$ ),  $\Omega_{\text{arg}}$ , and pH (total scale) from TA and DIC using the CO2SYS v2.1 software [44]. We considered the carbonic acid dissociation constants  $K_1$  and  $K_2$  from Lueker [45], the acidity constant of the bisulfate ion from Dickson [46], and the boric acid constant from Uppstrom [47]. For the SE station, we used the boric acid constant from Lee [48], given that it is more suitable for higher pH values. The solubility constant used to derive the  $\Omega_{\text{arg}}$  is from Mucci [49].

### Air-sea $\text{CO}_2$ flux

The air-sea  $\text{CO}_2$  flux was estimated according to  $F = k S \Delta p\text{CO}_2$ , where  $F$  is the flux in  $\text{mmol m}^{-2} \text{day}^{-1}$ ,  $k$  is the gas transfer velocity ( $\text{m day}^{-1}$ ),  $S$  is the  $\text{CO}_2$  solubility coefficient according to Weiss [50], and  $\Delta p\text{CO}_2$  is the ocean surface and atmosphere  $p\text{CO}_2$  difference. We obtained the atmospheric  $p\text{CO}_2$  values from the Map $\text{CO}_2$  buoy in the Enrique Cay forereef (Fig 1). We considered the recent parametrization from Ho [52] that integrates horizontal current velocity, depth, and wind speed to calculate the gas transfer velocity. This parametrization works well

for this type of study since it considers any bottom-generated turbulence. We assumed a horizontal current velocity of  $5 \text{ cm s}^{-1}$  for the latter calculation, given that such magnitude is approximate from previous observations (unpublished results). Wind speed was measured at a 15-meter height and adjusted to a 10-meter wind [51].

### pH drivers and seasonality analysis

To assess the pH seasonality and its controlling mechanisms in BB, we calculated (using CO2SYS) the effects of temperature, salinity, TA, DIC, and air-sea DIC exchange on pH. The following equation describes observed monthly changes between time  $t_2$  and  $t_1$  (e.g., February and January) in pH ( $\Delta pH$ ), assuming that each process modified the carbonate system independently and that the water column is well mixed:

$$\Delta pH = \Delta pH(T) + \Delta pH(S) + \Delta pH(F) + \Delta pH(TA) + \Delta pH(DIC) + R \quad (1)$$

where the terms on the right-hand side of the equation correspond to changes in temperature (T), salinity (S), air-sea DIC exchange (F) in  $\text{CO}_2$  form, TA, DIC, and a residual (R), which represents the remainder of the difference between the terms of the right-hand side of Eq (1) and the observed pH changes ( $\Delta pH$ ). Differences in pH were between the initial ( $pH_{calc}$  at  $t_1$ ) and modified ( $pH_2$  at  $t_2$ ) conditions according to the following equations:

$$\Delta pH(T) = pH_2(T_2, S_1, TA_1, DIC_1) - pH_{calc} \quad (2)$$

$$\Delta pH(S) = pH_2(T_1, S_2, TA_1, DIC_1) - pH_{calc} \quad (3)$$

$$\Delta pH(TA) = pH_2(T_1, S_1, TA_2, DIC_1) - pH_{calc} \quad (4)$$

We refer to  $pH_1(T_1, S_1, DIC_1, TA_1)$  at  $t_1$  as  $pH_{calc}$ . Changes in DIC drive both  $\Delta pH(F)$  and  $\Delta pH(DIC)$ : the former term refers to DIC changes resulting from air-sea  $\text{CO}_2$  exchange, while the latter term includes DIC changes caused by both water-column and benthic mechanisms. To determine  $\Delta pH(F)$ , we first calculated the DIC change ( $\Delta DIC_{air-sea}$ ) using the  $\text{CO}_2$  air-sea exchange ( $F$ ,  $\text{mmol m}^{-2} \text{d}^{-1}$ ), seawater density ( $d$ ,  $\text{kg m}^{-3}$ ), change in time ( $t_2 - t_1$ , days), and sampled depth ( $H$ , m) [52]:

$$\Delta DIC_{air-sea} = \frac{-F \cdot (t_2 - t_1)}{d \cdot H} \quad (5)$$

$$\Delta pH(F) = pH_2(T_1, S_1, TA_1, DIC_1 + \Delta DIC_{air-sea}) - pH_{calc} \quad (6)$$

Given that changes in pH due to DIC include the effect of  $\text{CO}_2$  air-sea exchange, we subtracted  $\Delta pH(F)$  from  $\Delta pH(DIC)$  to separate both signals:

$$\Delta pH(DIC) = (pH_2(T_1, S_1, TA_1, DIC_2) - pH_{calc}) - \Delta pH(F) \quad (7)$$

## Results and discussion

### Carbonate chemistry spatio-temporal variability

We averaged all the interannual data from BB and SE to monthly values (Fig 4). Differences in salinity and temperature variabilities between BB and SE support the contention of limited exchange between BB and outer coastal waters [27, 53]. The exchange regime results from the semi-enclosed physiography and the small tidal range typical for the region. The larger magnitudes of temperature and salinity observed at BB are likely due to higher daytime evaporation rates [54]. Water temperature remained above  $29^\circ\text{C}$  at BB for most of the year, from May to

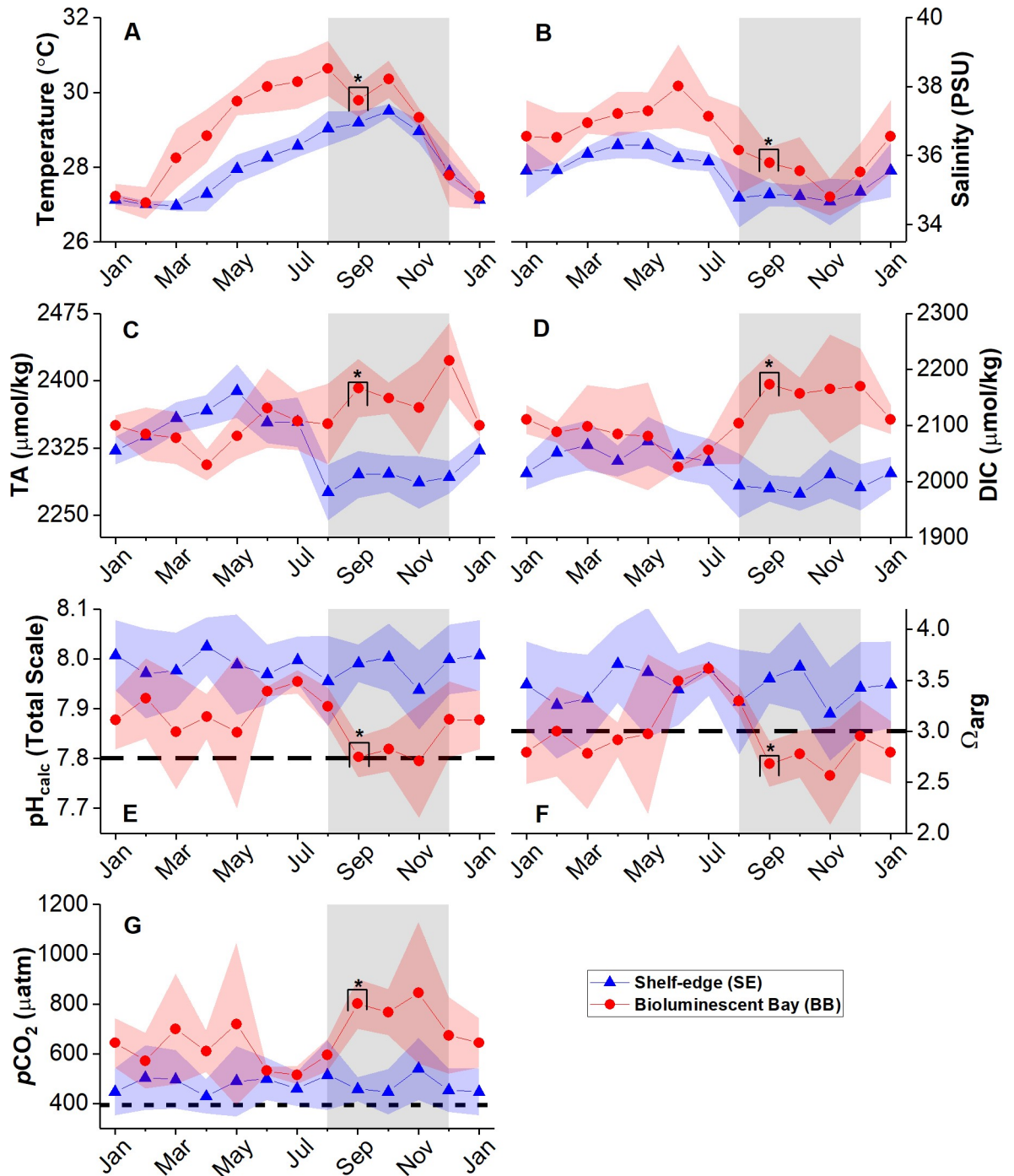


**Fig 4. Monthly mean carbonate chemistry parameters at BB and SE stations.** (A) Monthly mean temperature, (B) salinity, (C) TA, (D) DIC, (E)  $pH_{calc}$ , (F)  $\Omega_{arg}$  and (G)  $pCO_2$ . The long-dashed lines in (E) and (F) represent expected mean values by 2100 under business-as-usual scenarios (RCP 8.5) [55]. The short-dashed line in (G) is the mean atmospheric  $pCO_2$  value (394  $\mu atm$ ) during the sampling period. Red and blue shaded areas represent one standard deviation for each data point, while gray shades represent the wet season. For every averaged data point,  $n \geq 3$ . Data points depicted with an asterisk show where  $n = 3$ . Data are in S1 and S2 Tables.

<https://doi.org/10.1371/journal.pone.0250069.g004>

November. We detected the salinity minimums at both stations in November due to large amounts of accumulated precipitation (Fig 3B). The salinity decrease at SE after April was due to the influence of riverine water from the Amazon and Orinoco river plumes, later magnified

by the maximum outflow of the Orinoco in September [29, 30] and the start of the wet season in August (Fig 3B). June was the driest month during the sampling period and anomalously dry relative to climatological data. BB's higher salinities are due to its enclosed nature and the year-round dominance of evaporation [27] and evapotranspiration [54] over precipitation.

The data presented in Table 1 and Fig 4 show that BB was consistently more acidified (lower pH and  $\Omega_{\text{arg}}$ ) than SE throughout the year. The larger amplitudes observed in the BB data evidence a marked seasonality relative to the SE data. BB's pH values are near the projected 7.8 mean for 2100 under business-as-usual CO<sub>2</sub> scenarios (RCP 8.5) during September and November, while we often observed  $\Omega_{\text{arg}}$  below or near the 3.0 projected value [55].

BB's lower pH values coincided with higher TA concentrations (relative to SE), suggesting that the excess TA was insufficient to buffer the declines in pH and  $\Omega_{\text{arg}}$ . Thus, we observed an average excess (relative to the oceanic reference station, SE) of mean TA and DIC of + 36 and + 94  $\mu\text{mol kg}^{-1}$ , respectively. The mean seawater  $p\text{CO}_2$  (Fig 4G) at BB station was above the mean atmospheric  $p\text{CO}_2$  (400  $\mu\text{atm}$ ) year-round by approximately 270  $\mu\text{atm}$ .

As indicated by pH and  $\Omega_{\text{arg}}$  data, the acidification reaches its maximum at BB during the wet season when the mean pH decreased by 0.06 units, and the mean  $\Omega_{\text{arg}}$  decreased by 0.19. During that time (Aug-Nov), we observed an excess of mean TA and DIC of + 81 and + 152  $\mu\text{mol kg}^{-1}$ , respectively, relative to SE. Thus, mean TA and DIC in BB increased during the wet season by 15 and 48  $\mu\text{mol kg}^{-1}$ , which is not enough to induce a net buffering effect [7]. Also, we observed  $p\text{CO}_2$  values above 600  $\mu\text{atm}$ , thus 200  $\mu\text{atm}$  above the 400  $\mu\text{atm}$  atmospheric global means. This study provides the first characterization of the seasonal carbonate chemistry within a mangrove system in Puerto Rico. These results show that not all mangrove lagoons can buffer OA at seasonal time scales and serve to advance our understanding of the diverse roles mangroves may play in modulating acidification in tropical coastal environments.

### Influence of TA and DIC variability on pH and $\Omega_{\text{arg}}$

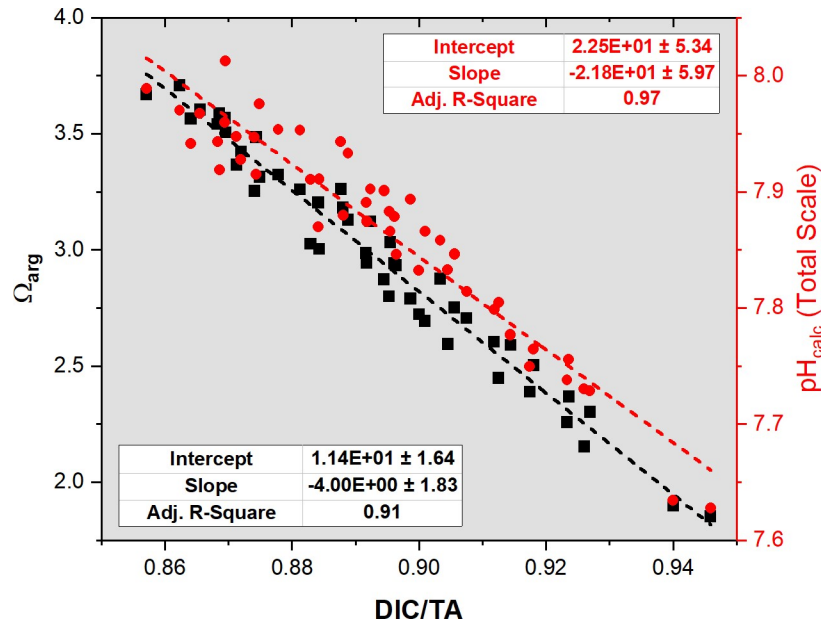
The relationship between DIC and TA can provide insights into the mechanisms that control OA [56]. Both  $\Omega_{\text{arg}}$  and  $\text{pH}_{\text{calc}}$  showed significant ( $p < 0.00001$ ;  $n = 47$ ) and strong correlations ( $R^2 = 0.97$  and  $0.91$ , respectively) with the DIC/TA ratio (Fig 5). This ratio evidences the sensitivity of the system to perturbations in dissolved seawater CO<sub>2</sub> concentration [57]. If the DIC

Table 1. Maximum and minimum monthly means ( $\pm$  one standard deviation) for each parameter from Fig 4.

| Observations                | SE         |            |            | BB         |            |            |
|-----------------------------|------------|------------|------------|------------|------------|------------|
|                             | Mean       | Maximum    | Minimum    | Mean       | Maximum    | Minimum    |
| Temperature                 | 28.19      | 29.51      | 26.97      | 29.03      | 30.64      | 27.04      |
| (°C)                        | $\pm 0.93$ | $\pm 0.18$ | $\pm 0.14$ | $\pm 1.36$ | $\pm 0.74$ | $\pm 0.42$ |
| Salinity                    | 35.42      | 36.31      | 34.66      | 36.47      | 38.01      | 34.81      |
|                             | $\pm 0.74$ | $\pm 0.38$ | $\pm 0.68$ | $\pm 1.14$ | $\pm 1.21$ | $\pm 0.54$ |
| TA                          | 2323       | 2389       | 2275       | 2359       | 2407       | 2306       |
| ( $\mu\text{mol kg}^{-1}$ ) | $\pm 42$   | $\pm 30$   | $\pm 31$   | $\pm 43$   | $\pm 57$   | $\pm 17$   |
| DIC                         | 2020       | 2072       | 1981       | 2114       | 2175       | 2035       |
| ( $\mu\text{mol kg}^{-1}$ ) | $\pm 49$   | $\pm 44$   | $\pm 29$   | $\pm 73$   | $\pm 108$  | $\pm 38$   |
| $\text{pH}_{\text{calc}}$   | 7.99       | 8.02       | 7.94       | 7.87       | 7.96       | 7.79       |
| (total scale)               | $\pm 0.07$ | $\pm 0.05$ | $\pm 0.08$ | $\pm 0.09$ | $\pm 0.02$ | $\pm 0.11$ |
| $\Omega_{\text{arg}}$       | 3.45       | 3.67       | 3.17       | 2.96       | 3.64       | 2.57       |
|                             | $\pm 0.43$ | $\pm 0.35$ | $\pm 0.46$ | $\pm 0.47$ | $\pm 0.07$ | $\pm 0.48$ |
| $p\text{CO}_2$              | 477        | 540        | 430        | 674        | 845        | 497        |
| ( $\mu\text{atm}$ )         | $\pm 101$  | $\pm 125$  | $\pm 63$   | $\pm 188$  | $\pm 284$  | $\pm 39$   |

<https://doi.org/10.1371/journal.pone.0250069.t001>





**Fig 5. Linear correlation of the DIC/TA ratio with pH and  $\Omega_{\text{arg}}$ .**

<https://doi.org/10.1371/journal.pone.0250069.g005>

to TA ratio equals 1, any addition/removal of  $\text{CO}_2$  (in the form of DIC) will result in a maximum decrease/increase of seawater pH and  $\Omega_{\text{arg}}$  [58], with soluble  $\text{CO}_2$  being more sensitive to temperature changes. Thus, TA and DIC changes controlled the pH decrease and  $\Omega_{\text{arg}}$  we observed in BB during the wet season (Fig 4).

When transitioning from the peak of the dry season (June–July) to the wet season (August–November), the mean DIC/TA ratio increased significantly ( $p < 0.001$ ,  $n = 6$  and 16, respectively) from  $0.87 \pm 0.00$  to  $0.91 \pm 0.02$ . At this time, we observed increases in DIC and TA of 100 and  $6 \mu\text{mol kg}^{-1}$ , respectively, decreasing pH and  $\Omega_{\text{arg}}$  by 0.12 and 0.75. Thus, the observed changes in water chemistry evidence that the increase of  $\text{CO}_2$  production (presumably from benthic and water column aerobic respiration) surpassed the increase of TA production from anaerobic processes, suggesting aerobic dominance over anaerobic remineralization. Sulfate reduction is an important TA producing reaction in tropical mangrove sediments [7, 21, 59, 60], while denitrification is not [7, 24, 61, 62]. Previously measured water column nitrate concentrations at BB were low ( $0.12 \mu\text{mol L}^{-1}$ , annual mean) and showed a limited seasonal variability [35]. Another study [24] in La Parguera reported low benthic denitrification ( $0.03$ – $0.35 \mu\text{mol m}^{-2} \text{h}^{-1}$ ) and nitrification ( $0.44$ – $3.15 \mu\text{mol m}^{-2} \text{h}^{-1}$ ) rates. However, we cannot rule out denitrification from occurring in the water column or the sediment–seawater interface. During the wet season, the salt flats to the north get flooded, and water flows into BB, possibly exporting nitrate and further enhancing denitrification [63].

Previous research (S3 Table) at BB reported that water column respiration exceeds primary production year-round. Aerobic respiration of organic matter releases essentially unbuffered DIC [9], given that it increases DIC by 1 mol and decreases TA by 0.2 moles for each mol of carbon oxidized (assuming a Redfield ratio). Previous work in mangrove environments has documented an increase in heterotrophic activity during the wet season [58, 61, 64], possibly fueled by carbon derived from allochthonous sources (i.e., phytoplankton, seagrass, terrestrial non-mangrove, or direct input of TA and DIC from runoff) or local sources (i.e., water column mechanisms or benthic mechanisms) [22, 59].

Studies have observed elevated concentrations of sulfide at bottom waters ( $1.6\text{--}3.5\text{ mmol L}^{-1}$ ) [32] and in porewaters ( $0.024\text{--}3.2\text{ mmol L}^{-1}$ ) [37] throughout the year. High sulfate reduction rates in BB ( $34.06\text{ mmol L}^{-1}\text{ h}^{-1}$ ) relative to an oceanic station located ca. 10 km from shore ( $9.33\text{ mmol L}^{-1}\text{ h}^{-1}$ ) were reported as well [37]. The higher sulfate reduction rates observed (see [37]) in BB indicate its potential role as a TA source, assuming minimal re-oxidation of reduced sulfur species [65, 66]. Sulfate reduction produces one mole of TA per mole of organic carbon oxidized, assuming that the sulfur species are not re-oxidized to sulfate [67].

### The drivers of the pH seasonality

The pH decomposition (Fig 6A) shows that seasonal changes were influenced the most by biological processes, given that  $\Delta pH(DIC)$  and  $\Delta pH(TA)$  exerted the most considerable changes to

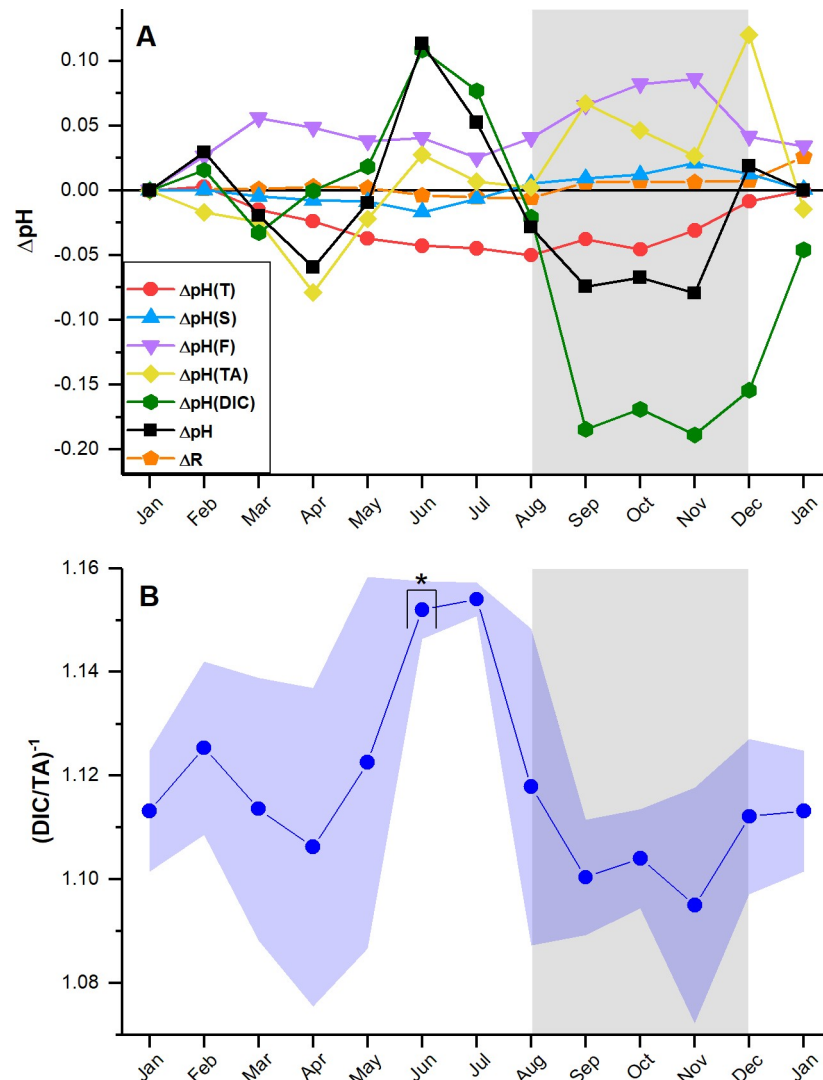


**Fig 6. Results of the pH decomposition.** (A) Cumulative monthly changes in pH (black line) due to temperature (red), salinity (blue),  $\text{CO}_2$  flux (violet), TA (yellow), and DIC (green). The analysis considered January as the starting point and added the changes from thereon. (B) Seasonal variability of the inverse DIC/TA ratio. The blue shade represents one standard deviation for each monthly mean. For each data point,  $n \leq 2$ . Data points depicted with an asterisk show where  $n = 2$ . The gray shades in both plots represent the wet season.

<https://doi.org/10.1371/journal.pone.0250069.g006>

monthly pH. The DIC/TA ratio (Fig 6B) closely follows the observed pH changes ( $\Delta\text{pH}$ ). Thus, the balance between changes in DIC and TA mainly modulated the pH variability. Increases in DIC decrease pH, while increases in TA increase pH. The mean annual magnitudes of  $\Delta\text{pH}(T)$  and  $\Delta\text{pH}(S)$  together equal 0.04, while the mean magnitudes of  $\Delta\text{pH}(DIC)$  and  $\Delta\text{pH}(TA)$  equal 0.08 and 0.04, respectively. Therefore, changes in pH due to mixing, dilution, and evaporation were the least significant. With a mean annual magnitude of 0.05, air-sea  $\text{CO}_2$  exchange increased pH ( $\Delta\text{pH}(F)$ ) year-round as expected [21]. When comparing the TA at BB with the TA at SE from March to May, we observe that the TA depleted in BB. Thus, some local processes must have consumed alkalinity. During the wet season, we observed the largest decrease in  $\Delta\text{pH}(DIC)$  and increase in  $\Delta\text{pH}(TA)$ , confirming that  $\text{CO}_2$  production from (presumably) aerobic respiration and TA production from anaerobic respiration increased at this time, while aerobic respiration dominated.

## Summary and conclusions

Results from this study evidence that BB could not buffer OA over a seasonal time frame. Although TA increased throughout the year, it was not enough to buffer the observed declines in pH and  $\Omega_{\text{arg}}$  resulting from increases in DIC. This acidification effect exacerbated during the wet season due to increased precipitation coinciding with more extensive tidal excursions (range), presumably enhancing the transport of labile organic matter into BB. Such an increase in heterotrophic activity during the wet season seems to be a general feature at La Parguera [68] enhanced in BB.

Given the insight gained in this study, future research should integrate temporal and diel surveys to better assess carbonate chemistry variability and trends at various time scales. It is unknown if the observed acidic conditions export to nearby environments (and to what extent) or if such conditions are detrimental to organisms other than corals. Future studies should couple the rates of benthic and water column remineralization processes with in-situ carbonate chemistry measurements. The chemistry and nutrient concentrations of runoff water should be measured as well. It is also essential to assess how the acidification discussed can impact organisms that live in the mangrove root systems and sediments.

## Supporting information

**S1 Fig. Mean tide level seasonality in meters at La Parguera.** Data frequency is one hour and corresponds to the sampling period (2014–18, top to bottom). Data are shown in blue, while the red line represents a third-degree polynomial fitting for each dataset. Gaps during the latter part of 2017 and the beginning of 2018 are due to the mareograph malfunctioning after Hurricane María (September 2017).

(TIF)

**S1 Table. Mean monthly data for all parameters measured at BB.**

(XLSX)

**S2 Table. Mean monthly data for all parameters measured at SE.**

(XLSX)

**S3 Table. Water column metabolic rates previously measured at BB.**

(PDF)

**S1 Dataset. Data corresponding to the BB station.**

(CSV)

**S2 Dataset. Data corresponding to the SE station.**  
(CSV)

## Acknowledgments

We are grateful to personnel and students from the Department of Marine Sciences (University of Puerto Rico–Mayagüez) who assisted during field and laboratory work. Thanks to Dr. Jorge Corredor and Carla Mejías for proofreading the manuscript. Thanks to Luis Pomales for helping to generate the maps of La Parguera and Bioluminescent Bay.

## Author Contributions

**Conceptualization:** Erick M. García-Troche, Julio M. Morell, Melissa Meléndez, Joseph E. Salisbury.

**Data curation:** Erick M. García-Troche.

**Formal analysis:** Erick M. García-Troche.

**Funding acquisition:** Julio M. Morell.

**Investigation:** Erick M. García-Troche, Melissa Meléndez.

**Methodology:** Erick M. García-Troche, Julio M. Morell, Melissa Meléndez, Joseph E. Salisbury.

**Project administration:** Erick M. García-Troche, Julio M. Morell.

**Resources:** Erick M. García-Troche, Julio M. Morell.

**Software:** Erick M. García-Troche, Melissa Meléndez.

**Supervision:** Erick M. García-Troche, Julio M. Morell, Melissa Meléndez, Joseph E. Salisbury.

**Validation:** Erick M. García-Troche, Melissa Meléndez.

**Visualization:** Erick M. García-Troche, Julio M. Morell, Melissa Meléndez, Joseph E. Salisbury.

**Writing – original draft:** Erick M. García-Troche.

**Writing – review & editing:** Erick M. García-Troche, Julio M. Morell, Melissa Meléndez, Joseph E. Salisbury.

## References

1. Camp EF, Schoepf V, Mumby PJ, Hardtke LA, Rodolfo-Metalpa R, Smith DJ, et al. The future of corals reefs subject to rapid climate change: Lessons from natural extreme environments. *Front Mar Sci*. 2018; 5(4): 1–21. <https://doi.org/10.3389/fmars.2018.00004>
2. Cheng L, Abraham J, Hausfather Z, Trenberth KE. How fast are the oceans warming? *Science*. 2018; 363(6423): 128–129. <https://doi.org/10.1126/science.aav7619> PMID: 30630919
3. Resplandy L, Keeling RF, Eddebbar Y, Brooks MK, Wang R, Bopp WL, et al. Quantification of ocean heat uptake from changes in atmospheric O<sub>2</sub> and CO<sub>2</sub> composition. *Nature*. 2018; 563: 105–108. <https://doi.org/10.1038/s41586-018-0651-8> PMID: 30382201
4. Hurd CL, Lenton A, Tilbrook B, Boyd PW. Current understanding and challenges for oceans in a higher-CO<sub>2</sub> world. *Nat Clim Chang*. 2018; 8: 686–694. <https://doi.org/10.1038/s41558-018-0211-0>
5. Intergovernmental Panel on Climate Change. *Climate Change 2014: Synthesis Report*. Geneva (Switzerland): World Meteorological Organization; 2015. 151 p.

6. Manzello DP, Enochs IC, Melo N, Gledhill DK, Johns EM. Ocean acidification refugia of the Florida Reef Tract. *Plos ONE*. 2012; 7(7): e41715. <https://doi.org/10.1371/journal.pone.0041715> PMID: 22848575
7. Sippo JZ, Maher DT, Tait DR, Holloway D, Santos IR. Are mangroves drivers or buffers of coastal acidification? Insights from alkalinity and dissolved inorganic carbon export estimates across a latitudinal transect. *Global Biogeochem Cycles*. 2016; 30(5): 753–766. <https://doi.org/10.1002/2015GB005324>
8. Yates KK, Rogers CS, Herlan JJ, Brooks GR, Smiley NA, Larson RA. Diverse coral communities in mangrove habitats suggest a novel refuge from climate change. *Biogeosciences*. 2014; 11: 4321–4337. <https://doi.org/10.5194/bg-11-4321-2014>
9. Thomas H, Schiettecatte LS, Suykens K, Koné YJM, Shadwick EH, Prowe AEF, et al. Enhanced ocean carbon storage from anaerobic alkalinity generation in coastal sediments. *Biogeosciences*. 2009; 6: 267–274. <https://doi.org/10.5194/bg-6-267-2009>
10. Unsworth RKF, Collier CJ, Henderson GM, McKenzie LJ. Tropical seagrass meadows modify seawater carbon chemistry: implications for coral reefs impacted by ocean acidification. *Environ Res Lett*. 2012; 7(2): 24026–24035. <https://doi.org/10.1088/1748-9326/7/2/024026>
11. Challenger RC, Robbins LL, McClintock JB. Variability of the carbonate chemistry in a shallow, seagrass-dominated ecosystem: implications for ocean acidification experiments. *Mar Freshw Res*. 2016; 67(2): 163–172. <https://doi.org/10.1071/MF14219>
12. Koweek DA, Zimmerman RC, Hewett KM, Gaylord B, Giddings S, Nickols KJ, et al. Expected limits on the ocean acidification buffering potential of a temperate seagrass meadow. *Ecol Appl*. 2018; 28(7): 1694–1714. <https://doi.org/10.1002/eap.1771> PMID: 30063809
13. Pacella SR, Brown CA, Waldbusser GG, Labiosa RG, Hales B. Seagrass habitat metabolism increases short-term extremes and long-term offset of CO<sub>2</sub> under future ocean acidification. *Proc Natl Acad Sci USA*. 2018; 115(15): 3870–3875. <https://doi.org/10.1073/pnas.1703445115> PMID: 29610330
14. Camp EF, Suggett DJ, Gendron G, Jompa J, Manfrino C, Smith DJ. Mangrove and seagrass beds provide different biogeochemical services for corals threatened by climate change. *Front Mar Sci*. 2016; 3(52): 1–16. <https://doi.org/10.3389/fmars.2016.00052>
15. Camp EF, Nitschke MR, Rodolfo-Metalpa R, Houlbreque F, Gardner SG, Smith DJ, et al. Reef-building corals thrive within hot-acidified and deoxygenated waters. *Sci Rep*. 2017; 7(2434). <https://doi.org/10.1038/s41598-017-02383-y> PMID: 28550297
16. Camp EF, Edmondson J, Doheny A, Rumney J, Grima AJ, Huete A, et al. Mangrove lagoons of the Great Barrier Reef support coral populations persisting under extreme environmental conditions. *Mar Ecol Prog Ser*. 2019; 625: 1–14. <https://doi.org/10.3354/meps13073>
17. Breithaupt JL, Smoak JM, Smith TJ, Hoare A, Sanders CJ. Organic carbon burial rates in mangrove sediments: Strengthening the global budget. *Global Biogeochem Cycles*. 2012; 26(3): GB3011. <https://doi.org/10.1029/2012GB004375>
18. Bouillon S, Dehairs F, Velimirov B, Abril G, Borges AV. Dynamics of organic and inorganic carbon across contiguous mangrove and seagrass systems (Gazi Bay, Kenya). *J Geophys Res Biogeosci*. 2007; 112(G2): G02018. <https://doi.org/10.1029/2006JG000325>
19. Golley F, Odum HT, Wilson RF. The structure and metabolism of a Puerto Rican red mangrove forest in May. *Ecology*. 1962; 43(1): 9–19. <https://doi.org/10.2307/1932034>
20. Bouillon S, Borges AV, Castañeda-Moya E, Diele K, Dittmar T, Duke NC, et al. Mangrove production and carbon sinks: a revision of global budget estimates. *Global Biogeochem Cycles*. 2008; 22(2): GB2013. <https://doi.org/10.1029/2007GB003052>
21. Borges AV, Djenidi S, Lacroix G, Théate J, Delille B, Frankignoulle M. Atmospheric CO<sub>2</sub> Flux from mangrove surrounding waters. *Geophys Res Lett*. 2003; 30(11): 1558. <https://doi.org/10.1029/2003GL017143>
22. Bouillon S, Dehairs F, Schiettecatte L, Viera Borges A. Biogeochemistry of the Tana Estuary and delta (northern Kenya). *Limnol Oceanogr*. 2007; 52(1): 46–59. <https://doi.org/10.4319/lo.2007.52.1.0046>
23. Krumins V, Gehlen M, Arndt S, Van Cappellen P, Regnier P. Dissolved inorganic carbon and alkalinity fluxes from coastal marine sediments: Model estimates for different shelf environments and sensitivity to global change. *Biogeosciences*. 2013; 10(1): 371–398. <https://doi.org/10.5194/bg-10-371-2013>
24. Mosquera AI, Corredor JE, Morell JM. Exponential collapse of benthic depurative capacity in a eutrophic tropical marine ecosystem: a threshold response to organic nitrogen loading. *Chem Ecol*. 1998; 14: 341–355. <https://doi.org/10.1080/02757549808037613>
25. Rivera-Monroy VH, Twilley RR, Boustany RG, Day JW, Vera-Herrera F, Ramírez MdC. Direct denitrification in mangrove sediments in a Terminos Lagoon, Mexico. *Mar Ecol Prog Ser*. 1995; 126(1–3): 97–109. <https://doi.org/10.3354/meps126097>

26. Balk M, Laverman AM, Keuskamp JA, Laanbroek HJ. Nitrate ammonification in mangrove soils: a hidden source of nitrite? *Front Microbiol.* 2015; 6(166): 1–10. <https://doi.org/10.3389/fmicb.2015.00166> PMID: 25784903
27. Margalef R. Hidrografía y fitoplancton de un área marina de la costa meridional de Puerto Rico. *Investigación Pesquera.* 1961; 18: 33–96.
28. Wüst G. Stratification and circulation in the Antillean-Caribbean Basins. 1st ed. Palisades (NY): Columbia University Press; 1964. 201 p.
29. Corredor JE, Morell JM. Seasonal variation of physical and biogeochemical features in eastern Caribbean Surface Water. *J Geophys Res.* 2001; 106(C3): 4517–4525. <https://doi.org/10.1029/2000JC000291>
30. López R, López JM, Morell J, Corredor JE, Del Castillo CE. Influence of the Orinoco River on the primary production of eastern Caribbean surface waters. *J Geophys Res Oceans.* 2013; 118(9): 4617–4632. <https://doi.org/10.1002/jgrc.20342>
31. Soler-Figueroa B, Otero E. The influence of rain regimes and nutrient loading on the abundance of two dinoflagellate species in tropical Bioluminescent Bay, Bahía Fosforescente, La Parguera, Puerto Rico. *Estuaries Coast.* 2015; 38(1): 84–92. <https://doi.org/10.1007/s12237-014-9827-0>
32. Cintrón G, Maddux WS, Burkholder PR. Some consequences of brine pollution in The Bahía Fosforescente, Puerto Rico. *Limnology and Oceanography.* 1970; 15(2): 246–249. <https://doi.org/10.4319/lo.1970.15.2.0246>
33. Vega M. Estimating primary productivity of red mangroves in southwestern Puerto Rico from remote sensing and field measurements [master's thesis]. [Mayagüez (PR)]: University of Puerto Rico at Mayagüez; 2008. 92 p.
34. Cintrón-Molero G. Seasonal fluctuations in a tropical bay [master's thesis]. [Mayagüez (PR)]: University of Puerto Rico at Mayagüez; 1969. 111 p.
35. Gonzalez JG. Primary productivity of the neritic and offshore waters of western Puerto Rico. Mayagüez (PR): Institute of Marine Sciences; 1965. 40p. Contract No.: NONR-4318(00). Supported by U.S. Office of Naval Research. 1967.
36. Burkholder PR, Burkholder LM. Studies on B vitamins in relation to productivity of the Bahía Fosforescente, Puerto Rico. *Bulletin of Marine Science of the Gulf and Caribbean.* 1958; 8(3): 201–223.
37. Otero E. Sulfate reduction rates in sediments of La Parguera, Puerto Rico: Effect of organic matter content and sediment characteristics [master's thesis]. [Mayagüez (PR)]: University of Puerto Rico at Mayagüez; 1988. 61 p.
38. Dickson AG, Sabine CL, Christian JR. Guide to best practices for ocean CO<sub>2</sub> measurements. Sidney (BC): North Pacific Marine Science Organization (Canada); 2007 Oct. 191 p. Report No.: 8 p.
39. Climate Data Online [Internet]. Asheville (NC): NOAA National Centers For Environmental Information; c2014 [cited 2018 Aug 6]. Available from: <https://www.ncdc.noaa.gov/cdo-web/datasets/GSOM/stations/GHCND:RQC00665693/detail>.
40. NOAA Tides & Currents [Internet]. Silver Spring: Center for Operational Oceanographic Products and Services (CO-OPS); c2014 [cited 2018 Oct 2]. Available from: <https://tidesandcurrents.noaa.gov/waterlevels.html?id=9759110>.
41. Gran G. Determination of the equivalence point in potentiometric titrations of seawater with hydrochloric acid. *Oceanol Acta.* 1952; 5: 209–218.
42. Dickson A, Afghan JD, Anderson GC. Reference materials for oceanic CO<sub>2</sub> analysis: A method for the certification of total alkalinity. *Marine Chemistry.* 2003; 80(2): 185–197. [https://doi.org/10.1016/S0304-4203\(02\)00133-0](https://doi.org/10.1016/S0304-4203(02)00133-0)
43. Cai WJ, Wang Y, Hodson RE. Acid-base properties of dissolved organic matter in the estuarine waters of Georgia, USA. *Geochim Cosmochim Acta.* 1998; 62(3): 473–483. [https://doi.org/10.1016/S0016-7037\(97\)00363-3](https://doi.org/10.1016/S0016-7037(97)00363-3)
44. Pierrot D, Lewis E, Wallace DWR. MS Excel Program Developed for CO<sub>2</sub> System Calculations. Oak Ridge, Tennessee: Carbon Dioxide Information Analysis Center, Oak Ridge National Laboratory, U.S. A Department of Energy; 2006. Report No.: ORNL/CDIAC-105a.
45. Lueker TJ, Dickson AG, Keeling CD. Ocean pCO<sub>2</sub> calculated from dissolved inorganic carbon, alkalinity, and equations for K<sub>1</sub> and K<sub>2</sub>: validation based on laboratory measurements of CO<sub>2</sub> in gas and seawater at equilibrium. *Mar Chem.* 2000; 70: 105–119. [https://doi.org/10.1016/S0304-4203\(00\)00022-0](https://doi.org/10.1016/S0304-4203(00)00022-0)
46. Dickson AG. Standard potential of the reaction: AgCl(s)+1/2H<sub>2</sub>(g) = Ag(s)+HCl(aq), and the standard acidity constant of the ion HSO<sub>4</sub> in synthetic sea water from 273.15 to 318.15 K. *J Chem Thermodyn.* 1990; 22(2): 113–127. [https://doi.org/10.1016/0021-9614\(90\)90074-Z](https://doi.org/10.1016/0021-9614(90)90074-Z)
47. Uppstrom LR. The boron/chlorinity ratio of deep-sea water from the Pacific Ocean. *Deep-Sea Res Oceanogr Abstr.* 1974; 21(2): 161–162. [https://doi.org/10.1016/0011-7471\(74\)90074-6](https://doi.org/10.1016/0011-7471(74)90074-6)

48. Lee K, Kim T, Byrne RH, Millero FJ, Feely RA, Liu Y. The universal ratio of boron to chlorinity for the North Pacific and North Atlantic oceans. *Geochimica et Cosmochimica Acta*. 2010; 74(6): 1801–1811. <https://doi.org/10.1016/j.gca.2009.12.027>
49. Mucci A. The solubility of calcite and aragonite in seawater at various salinities, temperatures and one atmosphere total pressure. *Am J Sci*. 1983; 283(7): 780–799. <https://doi.org/10.2475/ajs.283.7.780>
50. Weiss RF. Carbon dioxide in water and seawater: the solubility of a non-ideal gas. *Mar Chem*. 1974; 2(3): 203–215. [https://doi.org/10.1016/0304-4203\(74\)90015-2](https://doi.org/10.1016/0304-4203(74)90015-2)
51. Amoroch J, DeVries JJ. A new evaluation of the wind stress coefficient over water surfaces. *J Geophys Res*. 1980; 85(C1): 433–442. <https://doi.org/10.1029/JC085iC01p00433>
52. Xue L, Cai W, Hu X, Sabine C, Jones S, Sutton AJ, et al. Sea surface carbon dioxide at the Georgia time series site (2006–2007): Air-sea flux and controlling processes. *Prog Oceanogr*. 2016; 140: 14–26. <https://doi.org/10.1016/j.pocean.2015.09.008>
53. Selinger HH, Carpenter JH, Loftus M, Biggley WH, McElroy WD. Bioluminescence and phytoplankton successions in Bahía Fosforescente, Puerto Rico. *Limnol Oceanogr*. 1971; 16(4): 608–622. <https://doi.org/10.4319/lo.1971.16.4.0608>
54. Goyal MR. Potential evapotranspiration for the south coast of Puerto Rico with the Hargreaves-Samani technique. *The Journal of Agriculture of the University of Puerto Rico*. 1988; 72(1): 57–63. <https://doi.org/10.46429/jaupr.v72i1.6834>
55. Ricke KL, Orr JC, Schneider K, Caldeira K. Risks to coral reefs from ocean carbonate chemistry changes in recent earth system model projections. *Environ Res Lett*. 2013; 8(3): 1–6. <https://doi.org/10.1088/1748-9326/8/3/034003>
56. Xue L, Cai W. Total alkalinity minus dissolved inorganic carbon as a proxy for deciphering ocean acidification mechanisms. *Mar Chem*. 2020; 222: 1–10. <https://doi.org/10.1016/j.marchem.2020.103791>
57. Wang ZA, Wanninkhof R, Cai W, Byrne RH, Hu X, Peng T, et al. The marine inorganic carbon system along the Gulf of Mexico and Atlantic coasts of the United States: Insights from a transgressional coastal carbon study. *Limnol Oceanogr*. 2013; 58(1): 325–342. <https://doi.org/10.4319/lo.2013.58.1.0325>
58. Cotovicz LC, Knoppers BA, Brandini N, Poirier D, Costa-Santos SJ, Abril G. Aragonite saturation state in a tropical coastal embayment dominated by phytoplankton blooms (Guanabara Bay—Brazil). *Mar Pollut Bull*. 2017; 129(2): 729–739. <https://doi.org/10.1016/j.marpolbul.2017.10.064> PMID: 29102070
59. Alongi DM, Wattayakorn G, Pfitzner J, Tirendi F, Zagorskis I, Brunskill GJ, et al. Organic carbon accumulation and metabolic pathways in sediments of mangrove forests in southern Thailand. *Mar Geol*. 2001; 179(1–2): 85–103. [https://doi.org/10.1016/S0025-3227\(01\)00195-5](https://doi.org/10.1016/S0025-3227(01)00195-5)
60. Ho DT, Ferrón S, Engel VC, Anderson WT, Swart PK, Price RM, et al. Dissolved carbon biogeochemistry and export in mangrove-dominated rivers of the Florida Everglades. *Biogeosciences*. 2017; 14(9): 2543–2559. <https://doi.org/10.5194/bg-14-2543-2017>
61. Koné YJM, Borges AV. Dissolved inorganic carbon dynamics in the waters surrounding forested mangroves of the Ca Mau Province (Vietnam). *Estuar Coast Shelf Sci*. 2008; 77(3): 409–421. <https://doi.org/10.1016/j.ecss.2007.10.001>
62. Alongi DM, Tirendi F, Trott LA, Xuan TT. Benthic decomposition rates and pathways in plantations of the mangrove *Rhizophora apiculata* in the Mekong delta, Vietnam. *Mar Ecol Prog Ser*. 2000; 194: 87–101. <https://doi.org/10.3354/meps194087>
63. Hu X, Cai W. An assesment of ocean margin anaerobic processes on oceanic alkalinity budget. *Global Biogeochem Cycles*. 2011; 25(GB3003). <https://doi.org/10.1029/2010GB003859>
64. Hagens M, Slomp CP, Meysman FJR, Seitzinger SJB, Harlay J, Borges AV, et al. Biogeochemical processes and buffering capacity concurrently affect acidification in a seasonally hypoxic coastal marine basin. *Biogeosciences*. 2015; 12(5): 1561–1583. <https://doi.org/10.5194/bg-12-1561-2015>
65. Gustafsson E, Wällstedt T, Humborg C, Mörth C, Gustafsson BG. External total alkalinity loads versus internal generation: the influence of nonriverine alkalinity sources in the Baltic Sea. *Global Biogeochem Cycles*. 2014; 28: 1358–1370. <https://doi.org/10.1002/2014GB004888>
66. Rudd JWM, Kelly CA, Furutani A. The role of sulfate reduction in long term accumulation of organic and inorganic sulfur in lake sediments. *Limnol Oceanogr*. 1986; 31(6): 1281–1291. <https://doi.org/10.4319/lo.1986.31.6.1281>
67. Wolf-Gladrow DA, Zeebe RE, Klaas C, Körtzinger A, Dickson AG. Total alkalinity: The explicit conservative expression and its application to biogeochemical processes. *Marine Chemistry*. 2007; 106(1–2): 287–300. <https://doi.org/10.1016/j.marchem.2007.01.006>
68. Meléndez M, Salisbury J, Gledhill D, Langdon C, Morell JM, Manzello D, et al. Seasonal variations of carbonate chemistry at two western Atlantic coral reefs. *J Geophys Res Oceans*. 2020. <https://doi.org/10.1029/2020JC016108>